Evaluation of the theoretical uncertainties in the $Z \to \ell^+\ell^-$ cross sections at the LHC

Nadia E. Adam, Valerie Halyo and Scott A. Yost

Department of Physics, Princeton University,
Princeton, NJ 08544, U.S.A.
E-mail: `neadam@princeton.edu`, `valerieh@princeton.edu`, `syost@princeton.edu`

ABSTRACT: We study the sources of systematic errors in the measurement of the $Z \to \ell^+\ell^-$ cross-sections at the LHC. We consider the systematic errors in both the total cross-section and acceptance for anticipated experimental cuts. We include the best available analysis of QCD effects at NNLO in assessing the effect of higher order corrections and PDF and scale uncertainties on the theoretical acceptance. In addition, we evaluate the error due to missing NLO electroweak corrections and propose which MC generators and computational schemes should be implemented to best simulate the events.

Contents

1. Introduction

A precise measurement of gauge boson production cross-sections for pp scattering will be crucial at the LHC. W and Z bosons will be produced copiously, and a careful measurement of their production cross-sections will be important in testing the Standard Model more rigorously than ever before, and uncovering signs of new physics which may appear through radiative corrections. In addition, these cross-sections have been proposed as a "standard candle" for measuring the luminosity through a comparison of the measured rates to the best theoretical calculations of the cross-section. Investigation of this means of measuring luminosity began at the Tevatron and will continue at the LHC [1, 2].

In this paper, we will concentrate on Z production. A comparable analysis of systematic uncertainties in W production appeared in ref. [3]. Since that time, both the experimental approach to the measurements and the theoretical results needed to calculate them have both been refined. NNLO QCD calculations of these processes, previously available only for the total cross-section [4] and rapidity distribution [5], are now available in differential form [6], permitting an analysis of the effect of experimental cuts on the pseudorapidity and transverse momentum of the final state leptons.

The high luminosity ($10^{33} - 10^{34}$ cm^{2}s^{-1}) at the LHC insures that systematic errors will play a dominant role in determining the accuracy of the cross-section. Thus, we present an analysis of the effect of the theoretical uncertainty in the evaluation of the acceptance, and propose which among the various available MC generators and computational schemes should be implemented to best simulate the events.

This paper is organized as follows. Section 2 will give an overview of the calculation and the computational tools used in the analysis. The next four sections are each devoted

to estimating a class of systematic errors: electroweak corrections in section 3, NNLO QCD in section 4, QCD scale dependence in section 5, and parton distribution function uncertainties in section 6. Finally, the results are compiled and summarized in section 7.

2. Theoretical calculations and MC generators

The dominant production mechanism for Z bosons is the Drell-Yan process [7], in which a quark and antiquark annihilate to form a vector boson, which subsequently decays into a lepton pair. It is through this lepton pair $\ell^+\ell^-$ that the production process is observed. Such pairs may as well be produced via an intermediate photon γ^*, so both cases should be considered together. The Z production cross-section may be inferred experimentally from the number $N_{Z/\gamma^*}^{\mathrm{obs}}$ of observed events via the relation

$$N_{Z/\gamma^*}^{\mathrm{obs}} = \sigma^{\mathrm{tot}} \, \mathrm{BR}(Z/\gamma^* \to \ell^+\ell^-) A_{Z/\gamma^*} \int \mathcal{L}dt. \qquad (2.1)$$

A_{Z/γ^*} is the acceptance obtained after applying the experimental selection criteria. For example, if the cuts require $p_{\mathrm{T}}^\ell > p_{\mathrm{T}}^{\min}$, $0 < \eta^\ell < \eta_{\max}$, then

$$A_{Z/\gamma^*}(p_{\mathrm{T}}^{\min}, \eta_{\max}) = \frac{1}{\sigma^{\mathrm{tot}} \, \mathrm{BR}(Z/\gamma^* \to \ell^+\ell^-)} \int_{p_{\mathrm{T}}^{\min}}^{\sqrt{s}/2} \int_{-\eta_{\max}}^{\eta_{\max}} dp_{\mathrm{T}}^{\ell^+} \, dp_{\mathrm{T}}^{\ell^-} \, d\eta_{\ell^+} d\eta_{\ell^-}$$
$$\times \frac{d^4\sigma(pp \to Z/\gamma^* \to \ell^+\ell^-)}{dp_{\mathrm{T}}^{\ell^+} \, dp_{\mathrm{T}}^{\ell^-} \, d\eta_{\ell^+} d\eta_{\ell^-}}. \qquad (2.2)$$

In practice, further cuts on the invariant mass $M_{\ell\ell}$ of the lepton pair may be included to prevent the cross-section from being dominated by photons, which give a divergent contribution at low energies.

Alternatively to the Z production cross-section measurement, the corrected Z yield can be used as a standard candle for a luminosity monitor in LHC if one calculates the cross-section and solves for $\int \mathcal{L}dt$. The theoretical cross-section may be constructed by convoluting a parton-level cross-section $\widehat{\sigma}_{ab}$ for partons a and b with the parton density functions (PDFs) f_a, f_b for these partons,

$$\sigma^{\mathrm{th}}(pp \to Z/\gamma^* \to \ell^+\ell^-) = \sum_{a,b} \int_0^1 dx_1 dx_2 f_a(x_1) f_b(x_2) \, \widehat{\sigma}_{ab}(x_1, x_2), \qquad (2.3)$$

integrating over the momentum fractions x_1, x_2, and applying cuts relevant to the experiment. Theoretical errors come from limitations in the order of the calculation of σ_{ab}, on its completeness (for example, on whether it includes electroweak corrections or γ^*/Z interference, and on whether any phase space variables or spins have been averaged), and from errors in the PDFs.[1]

---

[1]The representation eq. 2.1 of the cross-section is intended to illustrate the manner in which the measurement may be used to infer the Z production cross-section, and does not imply that a narrow resonance approximation is actually used in calculating the cross-section 2.3.

Since the final state may include additional partons which form a shower, the output from the hard QCD process must be fed to a shower generator to generate a realistic final state seen in a detector. This is possible only if the cross-section is simulated in an event generator. Calculating the acceptance for all but the simplest cuts will normally require an event generator as well.

Thus, when constructing a simulation of an experiment, there is a range of choices which can be made among the tools currently available. An efficient calculation requires selecting those adequate to meet the anticipated precision requirements, without performing unnecessarily complex calculations. For example, while NNLO calculations are now available, the cross-sections are very complicated, do not always converge well, and require substantial time to calculate. For certain choices of cuts, it may be found that the effect of the NNLO result can be minimized, or that it can be represented by a simplified function for the parameters of interest. We will compare several possible schemes for calculating the Z production cross-section and acceptance, and consider the systematic errors arising for these schemes.

The most basic way to generate events is through one of the showering programs, such as PYTHIA [8], HERWIG [9], ISAJET [10] or SHERPA [11]. These vary somewhat in their assumptions and range of effects included, but they all start with hard partons at a high energy scale and branch to form partons at lower scales, which permits a description of hadronization and realistic events. On their own, these programs typically rely on a leading order hard matrix element and include only a leading-log resummation of soft and collinear radiation in the shower, limiting their value in describing events with large transverse momentum. In addition, ISAJET lacks color-coherence, which is important in predicting the correct distribution of soft jets [12].

Fully exclusive NLO QCD calculations are available for W and Z boson production [13]. The MC generator MC@NLO [14] combines a parton-level NLO QCD calculation with the HERWIG [9] parton shower, thus removing some of the limitations of a showering program alone.

Since $\alpha \approx \alpha_s^2$ at LHC energies, NLO electroweak (EWK) corrections should appear at the same order as NNLO QCD. The MC@NLO package is missing EWK corrections, but the most important of these corrections under the Z peak is expected to be QED final state radiation [17]. This can be obtained by combining MC@NLO with PHOTOS [15], an add-on program which generates multi-photon emission from events created by the host program. Another program, HORACE [18], is available which includes exact $\mathcal{O}(\alpha)$ EWK corrections together with a final state QED parton shower.

The other available NLO and NNLO calculations are implemented as MC integrations, which can calculate a cross-section but do not provide unweighted events. Some of these are more differential than others. For example, the NNLO rapidity distribution is available in a program Vrap [5], but this distribution alone is not sufficient to calculate acceptances with cuts on the lepton pseudorapidities and transverse momenta. A differential version of this NNLO calculation is implemented in a program FEWZ [6], but this is not an event generator. Another available program is ResBos-A [19], which resums soft and collinear initial state QCD radiation to all orders and includes NLO final state QED radiation. Re-

summation gives this program an advantage in realistically describing the small p_{T} regime.

Our analysis is conducted for di-lepton final states. The available calculations typically set the lepton masses to zero, so the lepton masses will be neglected throughout this paper and the choice of final state lepton has no effect on the calculations. In all results, ℓ may be interpreted as either an electron or muon. We have chosen three sets of experimental cuts to reflect detector capabilities and to demonstrate the impact of physics effects on the acceptances depending on the selection criteria.

3. Electroweak corrections

As noted above, both NNLO QCD corrections and NLO electroweak (EWK) corrections are expected to be needed to reach precisions on the order of 1% or better in Z boson production. NLO electroweak [20] and QCD corrections [13] are known both for W boson production and Z boson production. However, current state-of-the-art MC generators do not include both sets of corrections. The generator MC@NLO [14] combines a MC event generator with NLO calculations of rates for QCD processes and uses the HERWIG event generator for the parton showering, but it does not include EWK corrections. Final state QED can be added using PHOTOS [15, 16], a process-independent module for adding multi-photon emission to events created by a host generator. However, some $\mathcal{O}(\alpha)$ EWK corrections are still missing.

To study the error arising from missing $\mathcal{O}(\alpha)$ EWK corrections, we used HORACE [18], a MC event generator that includes initial and final-state QED radiation in a photon shower approximation and exact $\mathcal{O}(\alpha)$ EWK corrections matched to a leading-log QED shower. To determine the magnitude of the error, we then compared the results from this generator to a Born-level calculation with final-state QED corrections added by PHOTOS.

Specifically, we compared $pp \to Z/\gamma^* \to \ell^+\ell^-$ events generated by HORACE with the full O(α) corrections and parton-showered with HERWIG, to these events generated again by HORACE, but without EWK corrections (Born-level), showered with HERWIG+PHOTOS. CTEQ6.5M parton distribution functions [21] were used in the calculations. The results are shown in table 1 and in figures 1–3.

For table 1, the events are generated in the kinematic region defined by final state invariant mass $M_{\ell\ell} > 40$ GeV/c^2, and for each lepton, $p_T^\ell > 5$ GeV/c, and $|\eta_\ell| < 50.0$. Two sets of cuts are used:

Loose Cut : $\qquad M_{\ell\ell} > 40\,GeV/c^2$, $\qquad\qquad p_{\mathrm{T}}^\ell > 5\,GeV/c$, $\qquad |\eta_\ell| < 50.0$,

Tight Cut : $\qquad 40 < M_{\ell\ell} < 140\,GeV/c^2$, $\qquad p_{\mathrm{T}}^\ell > 20\,GeV/c$, $\qquad |\eta_\ell| < 2.0$.

The first row in the table shows the total generator-level cross-sections before QCD parton showering (identified by the label "No PS"). At Born level, without the corrections, the "loose" cut is essentially identical to the generator-level cut. The Born+FSR column shows the effect of applying final state radiation (FSR) corrections only via PHOTOS. In PHOTOS, FSR affects the rates through the cuts only. As noted in ref. [16], the combined effect of the complete first order real and virtual corrections not included in the standard

Photonic and Electroweak Corrections

	Born	Born+FSR	ElectroWeak	Difference
σ (No PS)	1984.2 ± 2.0	1984.2 ± 2.0	1995.7 ± 2.0	$0.58 \pm 0.14\%$
σ (Loose Cut)	1984.2 ± 2.0	1964.6 ± 2.0	1961.4 ± 2.0	$0.16 \pm 0.14\%$
σ(Tight Cut)	612.5 ± 1.1	597.6 ± 1.1	595.3 ± 1.1	$0.38 \pm 0.26\%$
A (Loose Cut)	0.9999 ± 0.0000	0.9901 ± 0.0001	0.9828 ± 0.0001	$0.74 \pm 0.02\%$
A (Tight Cut)	0.3087 ± 0.0005	0.3012 ± 0.0005	0.2983 ± 0.0005	$0.96 \pm 0.21\%$

Table 1: Calculation of the $Z/\gamma^* \to \ell^+\ell^-$ cross-section σ and acceptance A for various EWK corrections generated using HORACE 3.1, for $\ell = e$ or μ.
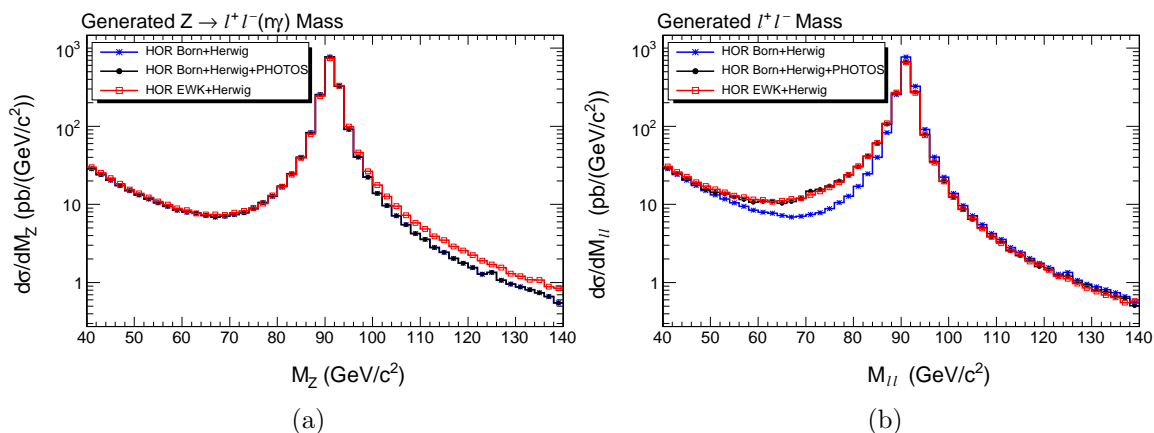

Figure 1: Comparison of the (a) Z boson invariant mass distributions and (b) $\ell^+\ell^-$ invariant mass distributions for the process $Z/\gamma^* \to \ell^+\ell^-(n\gamma)$ in HORACE 3.1 including $\mathcal{O}(\alpha)$ EWK corrections showered with HERWIG (open red squares), HORACE Born-level showered with HERWIG plus PHOTOS (black circles), and HORACE Born-level (blue stars).

version of PHOTOS would increase the total rate by a factor of $1 + 3\alpha/4\pi$, a 0.17% increase. The ElectroWeak column includes the full HORACE EWK corrections. In the final column, we give the difference between the previous two columns, to compare the full EWK correction FSR alone. The results show agreement within 1% between the two schemes. The maximum error in the cross-section is 0.58% without added parton shower, and the maximum error in the acceptance is 0.96% for the tighter cut. Therefore, we recommend using MC@NLO interfaced with PHOTOS as our primary event generator for measurements at the Z peak, until higher precision is required [17].

For completeness, we also compared MC@NLO interfaced with PHOTOS with distributions from ResBos-A [19], a MC simulation that includes final state NLO QED corrections to W/Z boson production and higher-order logarithmic resummation of soft and collinear QCD radiation. Figure 4 shows the distributions for $M_{\ell\ell}$ and the p_{T} of the Z boson, respectively. The latter exhibits especially well the effects of the soft and collinear resummation at low p_{T} in ResBos-A [19]. The only generator-level cut used in these comparison plots is the $M_{\ell\ell} > 50\,\mathrm{GeV}/c^2$. Otherwise, the default parameters were used with
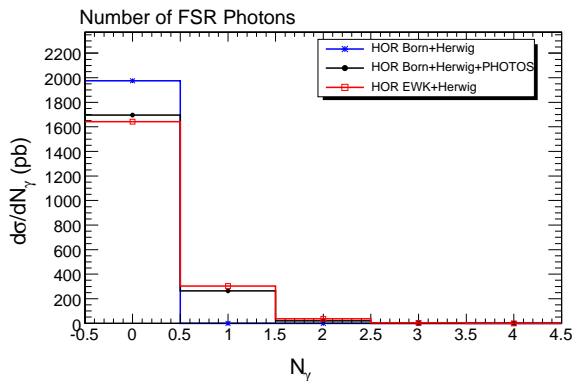
Number of FSR Photons

Figure 2: Comparison of the number n of final state radiation (FSR) photons in $Z/\gamma^* \to \ell^+\ell^-(n\gamma)$ for HORACE 3.1 including $\mathcal{O}(\alpha)$ EWK corrections showered with HERWIG (open red squares), HORACE Born-level showered with HERWIG plus PHOTOS (black circles), and HORACE Born-level (blue stars).
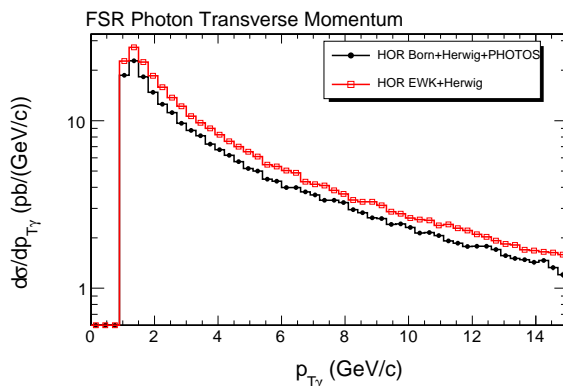
FSR Photon Transverse Momentum

Figure 3: Comparison of $Z/\gamma^* \to \ell^+\ell^-(n\gamma)$ final state radiation (FSR) transverse momentum distributions for HORACE 3.1 including EWK corrections showered with HERWIG (open red squares) and HORACE Born-level showered with HERWIG plus PHOTOS (black circles).

	Invariant Mass (GeV/c^2)	Pseudorapidity	Transverse Momentum (GeV/c)
Cut 1	$M_{\ell\ell} > 40$	$|\eta_\ell| < 2.0$	$p_T^\ell > 20$
Cut 2	$M_{\ell\ell} > 40$	$1.5 < |\eta_\ell| < 2.3$	$p_T^\ell > 20$
Cut 3	$79 < M_{\ell\ell} < 104$	$|\eta_\ell| < 2.0$	$p_T^\ell > 20$

Table 2: Acceptance regions for final state leptons in NNLO studies

no tuning.

4. NNLO QCD uncertainties

QCD uncertainties include errors due to missing higher-order corrections in the hard matrix
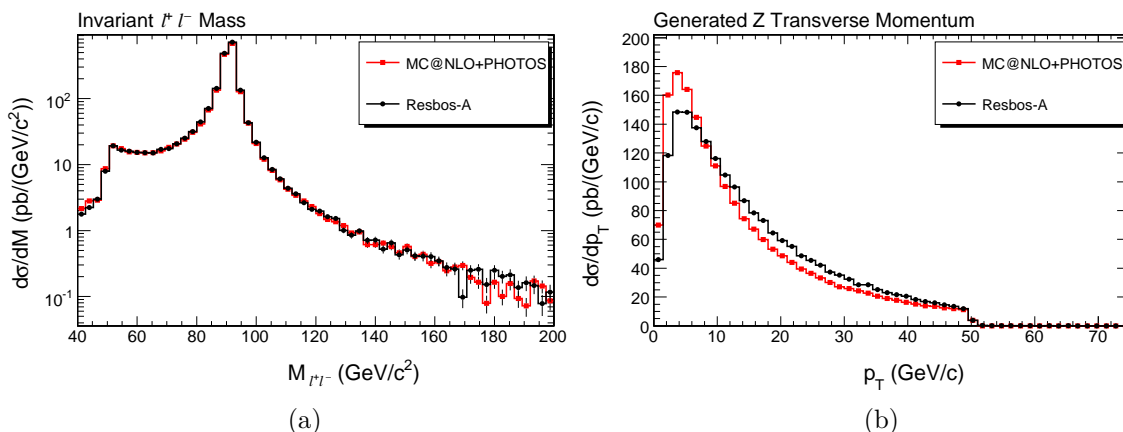
Figure 4: Comparison of the (a) di-lepton invariant mass and (b) Z transverse momentum distributions for the process $Z/\gamma^* \to \ell^+\ell^-(n\gamma)$, in MC@NLO with PHOTOS (red squares) and Resbos-A (black circles).

element, uncertainties in the parton distribution functions, and approximations made in the showering algorithms. In the following, we will evaluate the errors introduced by omitting the NNLO corrections by using MC@NLO, and calculate K-factors which can be used to introduce NNLO corrections to the MC@NLO calculation. We will also examine the effect of uncertainties in the PDFs. For these studies, we choose three sets of experimental cuts 2 to reflect detector capabilities and to demonstrate the impact of physics effects on the acceptances depending on the selection criteria. Here, η_ℓ and p_{T}^ℓ are the pseudorapidity and transverse momentum of the final state leptons. The different rapidity ranges and invariant di-lepton mass cuts provide useful separation for between regions of the Z spectrum which have different sensitivities to some of the sources of uncertainties and evaluate the impact of mass cut on the theoretical error.

We begin by examining the NNLO corrections, using the state-of-the-art program FEWZ [6], which is differential in the di-lepton invariant mass, and the lepton transverse momenta and pseudorapidities. The FEWZ program is at NNLO in perturbative QCD, and fully differential, giving correct acceptances including spin correlations, as well as taking into account finite widths effects and $\gamma^* - Z$ interference. Since we are interested primarily in studies about the Z peak, we choose the renormalization and factorization scales to be $\mu_F = \mu_R = M_Z$. Scale dependence will be discussed in detail the next section.

A comparison of the effects of higher order QCD corrections on the cross-section and acceptance is presented in table 3 and figures 5 – 7. Both the NLO and NNLO calculations are done with CTEQ6.5M PDFs [21]. We comment further on this choice at the end of this section. All results in the table are calculated at scale M_Z. In the figures, the NLO results are displayed as a band spanning the range of scales from $M_Z/2$ to $2M_Z$. The scale dependence of the NNLO result is small enough to be comparable to the precision of the

MC evaluation of the integrals, so only the average of the high and low scales is plotted, with error bars reflecting a combination of statistical and scale variation uncertainties.

NNLO Cross sections σ (pb)

Cut	MC@NLO	FEWZ NLO	FEWZ NNLO	K-factor	$K\times$ MC@NLO
σ^{tot}	2331 ± 3	2358.1 ± 2.3	2334.9 ± 4.6	0.9902 ± 0.0022	2308 ± 6
1	703.6 ± 1.1	716.0 ± 0.7	726.2 ± 5.5	1.0142 ± 0.0077	713.6 ± 5.6
2	71.3 ± 0.3	74.1 ± 0.07	73.39 ± 1.96	0.9902 ± 0.0280	70.6 ± 1.9
3	623.5 ± 1.0	657.2 ± 0.7	650.4 ± 4.0	0.9897 ± 0.0062	617.1 ± 4.0

NNLO Acceptances (%)

Cut	MC@NLO	FEWZ NLO	FEWZ NNLO	K-factor	$K\times$ MC@NLO
1	30.18 ± 0.06	30.36 ± 0.04	31.10 ± 0.24	1.0243 ± 0.0081	30.92 ± 0.25
2	3.06 ± 0.01	3.143 ± 0.004	3.143 ± 0.084	1.0000 ± 0.0268	3.06 ± 0.08
3	26.75 ± 0.06	27.87 ± 0.04	27.86 ± 0.18	0.9995 ± 0.0066	26.73 ± 0.19

Table 3: Calculation of the $Z/\gamma^* \to \ell^+\ell^-$ ($\ell = e$ or μ) cross-section at NLO using MC@NLO, and at NLO and NNLO using FEWZ, for the cut region defined in table 2. The acceptances are relative to a total generated cross-section $\sigma^{\rm tot}$ for $M_{\ell\ell} > 40\,{\rm GeV}/c^2$.
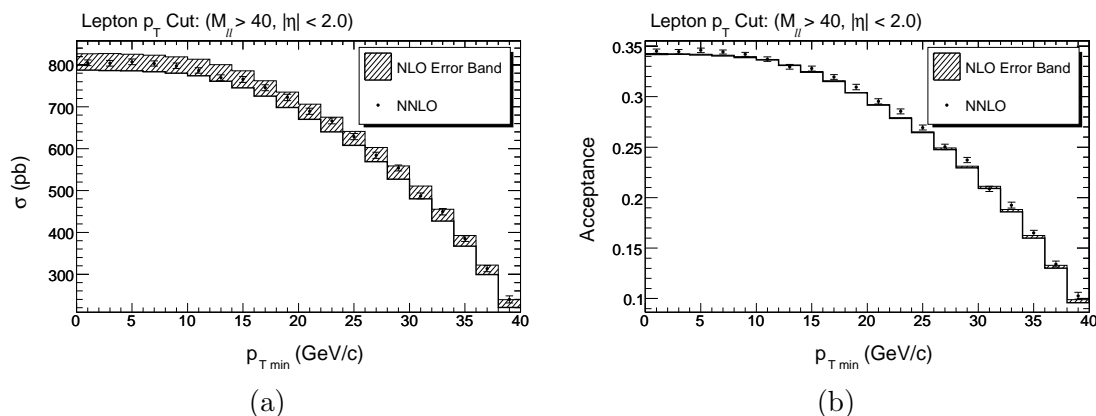

Figure 5: Cross-section (a) and acceptance (b) versus cut on lepton $p_{\rm T}$ at NLO (hashed bands) and NNLO (points), as calculated using FEWZ.

Figure 7 shows the cross-section and acceptance for an invariant mass band of width $\Delta M_{\ell\ell}$ centered at M_Z, to study the effect of selecting different cuts about the Z peak.

Since the NNLO matrix element has not yet been interfaced to a shower, we cannot directly compare FEWZ to MC@NLO. The best we can do at this time is to use MC@NLO to obtain the NLO showered result, and multiply this by a K-factor obtained by taking the ratio of the NNLO to NLO results derived from FEWZ. This procedure is reasonable except in threshold regimes where the fixed-order NLO result in FEWZ is unreliable. In fact, the NLO cross-section calculated by FEWZ can become negative near the threshold $p_{\rm T} = M_Z/2$. Similar methods have been used for calculating NNLO corrections to Higgs production [22]. The differences of these K-factors from unity are shown in figure 8 for both the cross-sections and acceptances, as a function of cuts on the lepton $p_{\rm T}$ and η as well as on the width $\Delta M_{\ell\ell}$ of an invariant mass cut centered at M_Z. The resulting accepted cross-section is shown in the $K\times$ MC@NLO column of table 3 and in figure 9 as a function
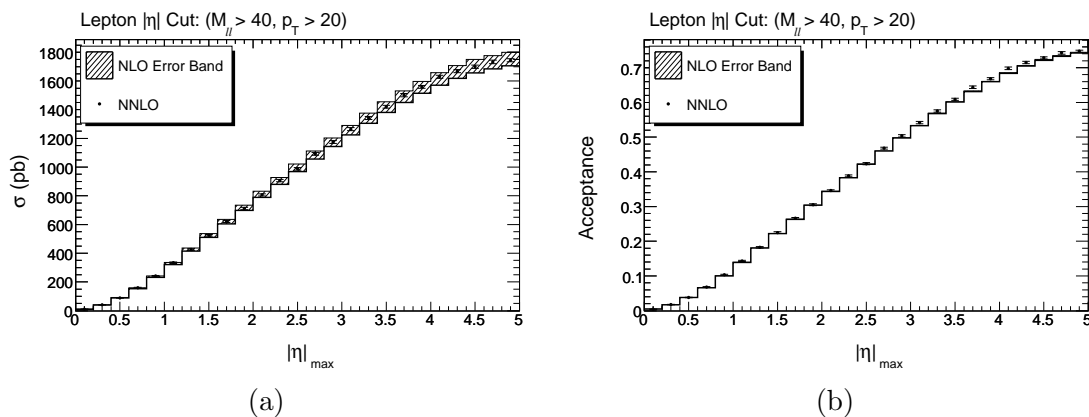
Figure 6: Cross-section (a) and acceptance (b) versus cut on lepton $|\eta|$ at NLO (hashed bands) and NNLO (points), as calculated using FEWZ.
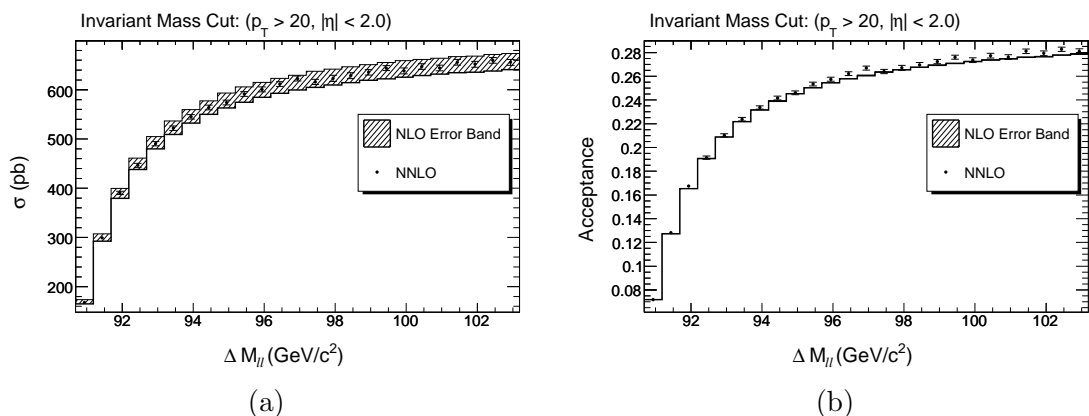

Figure 7: Cross-section (a) and acceptance (b) versus cut on di-lepton invariant mass $M_{\ell\ell}$, at NLO (hashed bands) and NNLO (points), as calculated using FEWZ. $M_{\ell\ell}$ is constrained to be in a band of width $\Delta M_{\ell\ell}$ centered at M_Z.

of the same cuts as in figure 8. The size of $K - 1$ is a good indicator of the error due to missing NNLO if MC@NLO is used without corrections.

The results in table 3 show K-factors corresponding to an NNLO correction of about 1% for the cross-sections, or up to 2.4% for the Cut 1 acceptance. FEWZ's convergence was not as good for Cut 2, however, leading to an almost 3% technical error in K from the evaluation.[2] In the other cases, a 1% evaluation of the NNLO correction was generally possible within a reasonable run time, which was typically of order one month on the clusters used in this study. Longer run times do not appear to improve the convergence significantly. The convergence limitations are due to the high dimensionality (11) of the Vegas [23] integrals and strong peaking of the integrands.

---

[2]Here, "technical error" refers to a limitation on the precision arising from the specific calculation of the process, rather than from the approximations made in the calculation at a theoretical level (NNLO vs. NLO, for example). Technical precision is discussed further in the conclusions.

Cut	CTEQ $K(\sigma)$	MRST $K(\sigma)$	CTEQ $K(A)$	MRST $K(A)$
1	1.0142 ± 0.0077	0.9963 ± 0.0109	1.0243 ± 0.0081	1.0211 ± 0.0113
2	0.9902 ± 0.0280	0.9830 ± 0.0348	1.0000 ± 0.0268	1.0074 ± 0.0357
3	0.9897 ± 0.0062	0.9851 ± 0.0082	0.9995 ± 0.0066	1.0096 ± 0.0087

Table 4: Comparison of the K factors for cross-sections and acceptances calculated using CTEQ6.5M (NLO) and MRST 2002 (NNLO) PDFs. $K(\sigma)$ is the K-factor for the cross-section and $K(A)$ is the K-factor for the acceptance, as displayed in table 3.

We should note that CTEQ6.5M structure functions were used in the above calculations because the K factors calculated are intended for rescaling an MC@NLO calculation using CTEQ PDFs. However, since these PDFs do not include NNLO corrections, it is useful to note the effect of repeating the calculations with MRST 2002 NNLO PDFs. The K-factors for the cross-section and acceptance for each of the three cuts is shown in table 4 for both sets of PDFs, for comparison. The $K(\sigma)$-factors are ratios of NNLO to NLO cross-sections, and $K(A)$ are ratios of NNLO to NLO acceptances relative to a total cross section for $M_{\ell\ell} > 40\,\text{GeV}$. Except for the cross-section K for Cut 1, where agreement is to 1.8%, the two PDF choices agree to within 1%, and within the computational uncertainty.

5. Scale dependence

Perturbative QCD calculations at fixed order depend on the factorization and renormalization scales introduced in the calculation. Thus, the previous calculations have an added uncertainty due to the choice of certain fictitious scales appearing in the calculation. In a complete, all order calculation, there would be no dependence on these scales. However, in a fixed order calculation matched to PDFs, a dependence on the factorization scale μ_F and renormalization scale μ_R appear in the final results. The effect of scale choice is significant at NLO. Adding NNLO effects is found to reduce scale dependence considerably [5, 6], though it can remain significant near thresholds where large logarithms render a fixed-order result unreliable.

As is customary, we will choose the renormalization and factorization scales to be identical, and investigate the scale dependence by varying them by a factor of 2 or 1/2 about a central value of $\mu_{F,R} = M_Z$, which is typical of the scales in our acceptance, and was the central value chosen in the previous section.

Table 3 included only the central scale M_Z. Tables 5 and 6 and show the total cross sections and acceptances for lepton production calculated by FEWZ at three different renormalization and factorization scales $M_Z/2$, M_Z, and $2M_Z$. The acceptances for the final state leptons are as defined in table 2. For a measure of the size of the scale dependence, the final column of each table shows the maximum difference between the three values divided by average, with an error calculated assuming the statistical errors in the three MC runs in each row are independent.

We can see that the scale dependence of the cross-sections at NLO is typically of order $\pm 2.5\%$. The scale dependence of NLO acceptances is dramatically reduced due to
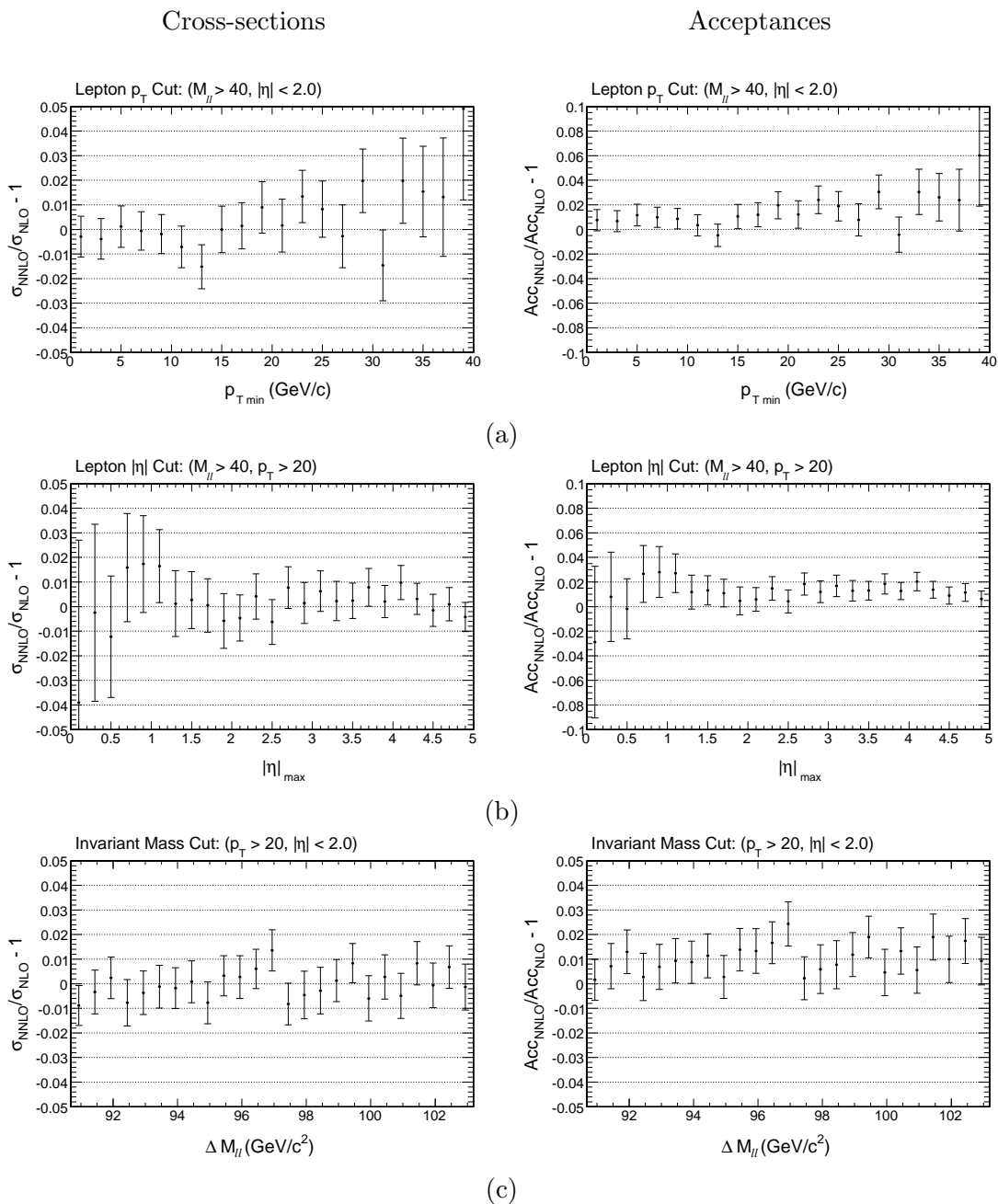
Figure 8: Fractional difference in the NNLO and NLO cross-sections (left-hand side) and acceptances (right-hand side) as a function of the lepton (a) $p_{\rm T}$, (b) $|\eta|$, and (c) $M_{\ell\ell}$ cuts as in figures 5–7. These differences are the factor $K - 1$ for the cross-section and acceptances, respectively.

correlations in the scale dependence of the cut and uncut cross-sections used to compute it. Adding NNLO reduces the scale dependence of the cross-sections to $\pm 1.2\%$ or less. These estimates were obtained using the CTEQ6.5M NLO PDFs, but are compatible with the scale dependence found using MRST 2002 NNLO PDFs for the same calculations, within the limits of the computational errors. A better evaluation of the NNLO result
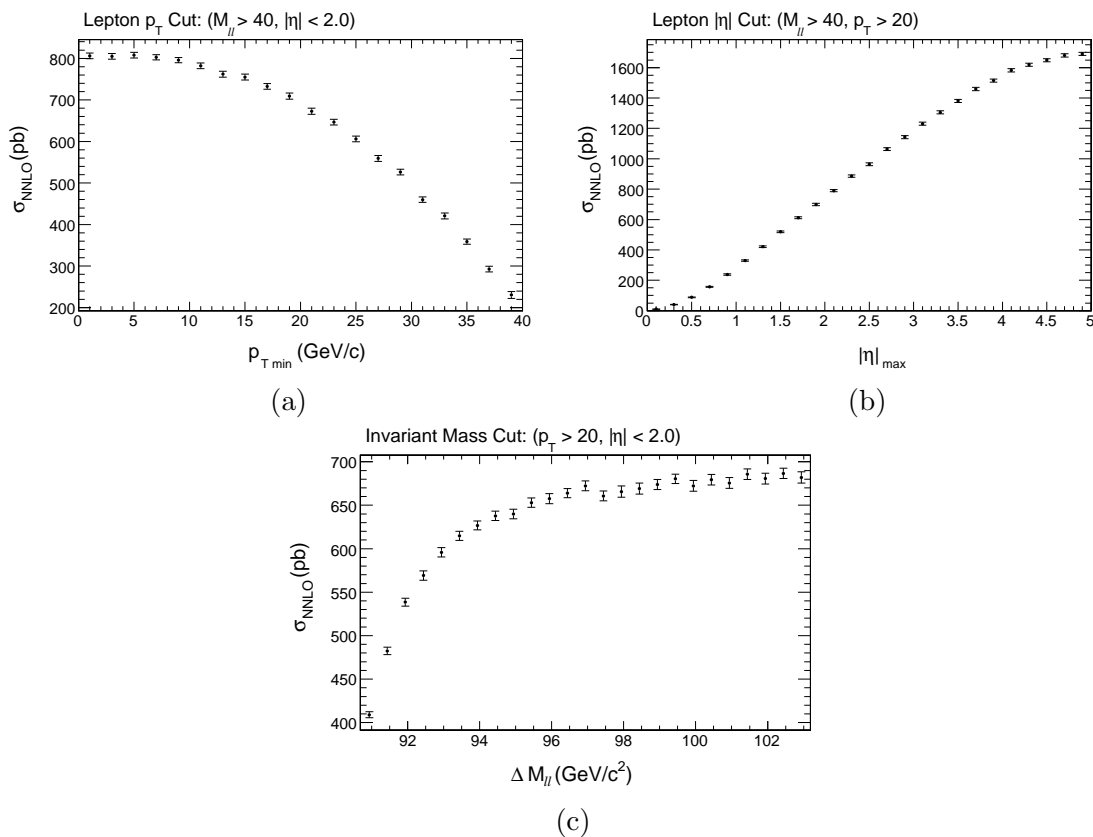
Figure 9: Accepted NNLO cross-section estimated from MC@NLO scaled by the K-factor versus the lepton (a) p_{T}, (b) $|\eta|$, and (c) $M_{\ell\ell}$ cuts as in figures 5–8.

may show the scale dependence to be even smaller, since it is at the same level as the MC precision. This is particularly true for Cut 2, for large values of $|\eta|$, where the cross-section is relatively small and the MC errors relatively large. Improving the convergence of FEWZ would reduce these errors.

6. Uncertainties due to the parton distribution function

Phenomenological parameterizations of the PDFs are taken from a global fit to data. Therefore, uncertainties on the PDFs arising from diverse experimental and theoretical sources will propagate from the global analysis into the predictions for the W/Z cross-sections. Figure 10 shows the results of the inclusive Z to di-lepton production cross-section using various CTEQ [21] and MRST [24] PDFs. The upward shift of about 7% (between CTEQ6.1 and 6.5 and MRST2004 and 2006) results from the inclusion of heavy quark effects in the latest PDF calculations. The acceptance due to the cuts in table 2 using each of these PDFs is shown in figure 11.[3]

---

[3]Some theoretical issues which may affect the contribution of the PDFs to the NNLO K-factor are not included here as we are concerned primarily with the error at NLO. See refs. [25] for details. The comparison at the end of section 4 suggests that such effects are likely to be small in the K factors calculated here.

Total Cross-section (in pb), $M_{\ell\ell} > 40\,\mathrm{GeV}$

Order	$M_Z/2$	M_Z	$2M_Z$	$\Delta\sigma/\overline{\sigma}$
NLO	2297.4 ± 2.3	2358.1 ± 2.3	2418.3 ± 2.3	0.0513 ± 0.0014
NNLO	2320.4 ± 4.6	2334.9 ± 4.6	2350.1 ± 4.6	0.0127 ± 0.0028

Cut Region 1

Order	$M_Z/2$	M_Z	$2M_Z$	$\Delta\sigma/\overline{\sigma}$
NLO	698.2 ± 0.7	716.0 ± 0.7	735.2 ± 0.7	0.0516 ± 0.0014
NNLO	718.9 ± 6.1	726.2 ± 5.5	719.8 ± 4.8	0.0101 ± 0.0108

Cut Region 2

Order	$M_Z/2$	M_Z	$2M_Z$	$\Delta\sigma/\overline{\sigma}$
NLO	72.55 ± 0.07	74.12 ± 0.07	75.78 ± 0.08	0.0436 ± 0.0014
NNLO	73.78 ± 2.00	73.39 ± 1.96	75.10 ± 1.52	0.0231 ± 0.0351

Cut Region 3

Order	$M_Z/2$	M_Z	$2M_Z$	$\Delta\sigma/\overline{\sigma}$
NLO	640.2 ± 0.6	657.2 ± 0.7	673.9 ± 0.7	0.0513 ± 0.0014
NNLO	661.3 ± 4.7	650.4 ± 4.0	656.2 ± 3.8	0.0166 ± 0.0090

Table 5: Scale dependence of the total and accepted cross-sections (in pb) for Z boson production with $M_{\ell\ell} > 40\,\mathrm{GeV}/c^2$ calculated by the FEWZ program at order NLO and NNLO. The final column is a measure of scale dependence obtained by dividing the maximum spread by the average for the three points.

Cut Region 1 (% Accepted)

Order	$M_Z/2$	M_Z	$2M_Z$	$\Delta A/\overline{A}$
NLO	30.39 ± 0.04	30.36 ± 0.04	30.40 ± 0.04	0.0013 ± 0.0020
NNLO	30.98 ± 0.27	31.10 ± 0.21	30.40 ± 0.04	0.0153 ± 0.0111

Cut Region 2 (% Accepted)

Order	$M_Z/2$	M_Z	$2M_Z$	$\Delta A/\overline{A}$
NLO	3.158 ± 0.031	3.143 ± 0.030	3.134 ± 0.033	0.0077 ± 0.0020
NNLO	3.180 ± 0.086	3.143 ± 0.084	3.196 ± 0.065	0.0165 ± 0.0353

Cut Region 3 (% Accepted)

Order	$M_Z/2$	M_Z	$2M_Z$	$\Delta A/\overline{A}$
NLO	27.87 ± 0.04	27.87 ± 0.04	27.87 ± 0.04	0.0001 ± 0.0020
NNLO	28.50 ± 0.21	27.86 ± 0.18	27.92 ± 0.17	0.0229 ± 0.0095

Table 6: Scale dependence of the acceptances A in the various cut regions for Z boson production with $M_{\ell\ell} > 40\,\mathrm{GeV}/c^2$ calculated by the FEWZ program at order NLO and NNLO. The final column is a measure of scale dependence obtained by dividing the maximum spread of the three preceding columns by their average.

The uncertainties in the PDFs arising from the experimental statistical and systematic uncertainties, and the effect on the production cross-section of the Z boson, have been studied using the standard methods proposed in refs. [21, 24]. For the standard set of
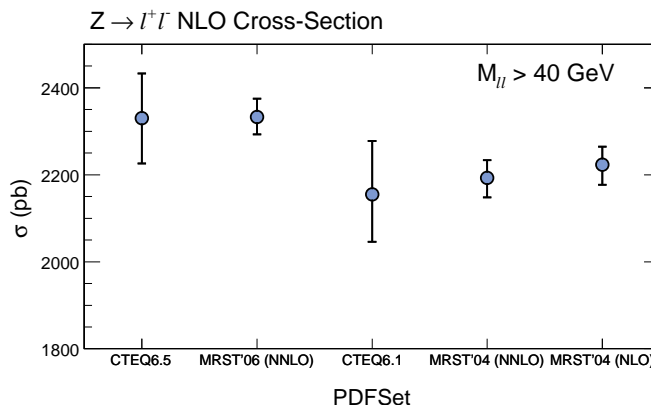
Figure 10: Comparison of $Z/\gamma^* \to \ell^+\ell^-$ cross-sections for $M_{\ell\ell} > 40\,\mathrm{GeV}/c^2$ for several recent PDF calculations.

PDFs, corresponding to the minimum in the PDF parameter space, a complete set of eigenvector PDF sets, which characterize the region nearby the minimum and quantify its error, have been simultaneously calculated. From the minimum set and these "error" sets we calculate the best estimate and the uncertainty for the Z cross-section. We do this using the asymmetric Hessian error method, [26] where the cross-section results from the various eigenvector PDF sets have been combined according to the prescriptions found in [21, 26]. Figure 10 list the results for the different PDFs and table 7 summarizes the results of the latest CTEQ and MRST PDF sets. These calculations were done using MC@NLO. The difference in the uncertainties (approximately a factor of two) between the results obtained from the CTEQ and MRST PDF error sets is due to different assumptions made by the groups while creating the eigenvector PDF sets. Note that the first column of table 3 should agree with the CTEQ6.5 entries in table 7, and do within the uncertainties quoted in table 3, although different event samples were used.

Finally we study the sensitivity of the kinematic acceptance calculations to the uncertainties affecting the PDF sets. Figures 12 and 13 show the systematic error on the production cross-sections as a function of the $|\eta|$ cut and minimum lepton p_{T} for variations on the three types of cuts in table 2. The fractional uncertainties, shown in in the same figures, demonstrate that the relative uncertainty in the cross-section is very flat as a function of the kinematic cuts, until the region of extreme cuts and low statistics in the MC are reached. The corresponding uncertainty on the acceptance as a function of the kinematic cuts is shown in figures 14 and 15. These show a similar dependence to the cross-section uncertainties, though the fractional errors are smaller.

7. Conclusions

To evaluate the overall contribution from theoretical uncertainties to both the cross-section and acceptance calculations for the decay mode $Z/\gamma^* \to \ell^+\ell^-$ ($\ell = e$ or μ) at the LHC (and for $M_{\ell\ell} > 40\,\mathrm{GeV}/c^2$) we add the uncertainties from each of the sources considered in the preceding sections. We compile the errors assuming that the calculation is done with

	$M_{\ell\ell} > 40\,\mathrm{GeV}/c^2$			Cut Region 1					
PDF Set	σ (pb)	$\Delta\sigma_+$	$\Delta\sigma_-$	σ (pb)	$\Delta\sigma_+$	$\Delta\sigma_-$	A	ΔA_+	ΔA_-
CTEQ6.5	2330	103	104	703.6	21.6	26.7	0.302	0.004	0.004
MRST2006	2333	42	40	712.6	13.6	16.0	0.305	0.004	0.004
CTEQ6.1	2155	123	109	652.1	30.2	29.5	0.303	0.007	0.005
MRST2004 (NNLO)	2193	41	45	672.4	12.6	17.9	0.302	0.004	0.004
MRST2004 (NLO)	2223	42	46	662.8	12.5	17.9	0.302	0.004	0.004
	$M_{\ell\ell} > 40\,\mathrm{GeV}/c^2$			Cut Region 2					
PDF Set	σ (pb)	$\Delta\sigma_+$	$\Delta\sigma_-$	σ (pb)	$\Delta\sigma_+$	$\Delta\sigma_-$	A	ΔA_+	ΔA_-
CTEQ6.5	2330	103	104	71.1	2.2	3.4	0.0305	0.0001	0.0005
MRST2006	2333	42	40	72.0	0.1	2.4	0.0308	0.0000	0.0010
CTEQ6.1	2155	123	109	66.3	3.0	4.1	0.0307	0.0006	0.0014
MRST2004 (NNLO)	2193	41	45	69.0	0.3	2.1	0.0310	0.0002	0.0007
MRST2004 (NLO)	2223	42	46	68.7	0.3	2.0	0.0313	0.0002	0.0007
	$M_{\ell\ell} > 40\,\mathrm{GeV}/c^2$			Cut Region 3					
PDF Set	σ (pb)	$\Delta\sigma_+$	$\Delta\sigma_-$	σ (pb)	$\Delta\sigma_+$	$\Delta\sigma_-$	A	ΔA_+	ΔA_-
CTEQ6.5	2330	103	104	623.5	20.8	22.0	0.268	0.005	0.003
MRST2006	2333	42	40	634.1	10.4	15.5	0.272	0.003	0.005
CTEQ6.1	2155	123	109	578.9	26.6	26.8	0.269	0.002	0.007
MRST2004 (NNLO)	2193	41	45	598.0	12.3	14.5	0.269	0.004	0.003
MRST2004 (NLO)	2223	42	46	588.5	12.1	14.3	0.268	0.004	0.003

Table 7: Cross-sections σ, and acceptances A, with asymmetric Hessian uncertainties as calculated using several recent PDF sets for the three cut regions defined in table 2.

MC@NLO at scale $\mu_F = \mu_R = M_Z$ and interfaced to PHOTOS to add final state QED radiation. The missing electroweak contribution may then be inferred from HORACE as in section 3. For these errors we take those resulting from the tight cut set in table 1; these cuts are considered the most representative of likely analysis cuts for the LHC experiments.

QCD uncertainties may be divided into two main classes. If the NNLO K-factor is set to 1, there is a missing NNLO contribution $\delta_{\mathrm{NNLO}} = K - 1$. Since K has residual NNLO scale dependence, we must also take this into account and write $K = 1 + \delta_{\mathrm{NNLO}} \pm \delta_{\mathrm{scale}}$. The factor δ_{NNLO} can be inferred from table 3 and δ_{scale} can be inferred from half the scale variation of the NNLO entries in table 5. For example, for the total cross-section, we can infer that $\delta_{\mathrm{NNLO}} = -(0.98 \pm 0.22)\%$, while $\delta_{\mathrm{scale}} = (0.64 \pm 0.16)\%$. Both errors in the MC@NLO result are of order 1%. The original NLO scale dependence estimate of 5.13% is no longer relevant because K is now known, even though it may be set to 1 in a particular calculation. Similar estimates can be made for the two sources of error in each of the cuts.

Both classes of QCD errors are also associated with a "technical precision" due to limitations of the computing tools used to evaluate them. Significant improvements in the NNLO precision could be obtained if a program with faster convergence were available. We therefore include an "error on the error" for the QCD errors, and propagate these through in the usual fashion to derive a final accuracy for the total QCD uncertainty estimate. This sets a limitation on how much the NLO calculation can realistically be improved using currently available NNLO results.

Cross-section $\Delta\sigma$				
Uncertainty	σ^{tot}	Cut 1	Cut 2	Cut 3
Missing NNLO	-0.98 ± 0.22	1.42 ± 0.77	-0.98 ± 2.80	-1.33 ± 0.62
Scale Dependence	0.64 ± 0.16	0.51 ± 0.54	1.16 ± 1.76	0.83 ± 0.46
Total	1.17 ± 0.20	1.51 ± 0.75	1.52 ± 2.25	1.57 ± 0.58
Error in Acceptance (ΔA)				
Uncertainty	$-$	Cut 1	Cut 2	Cut 3
Missing NNLO	$-$	2.43 ± 0.81	0.00 ± 2.68	-0.05 ± 0.66
Scale Dependence	$-$	0.77 ± 0.56	0.83 ± 1.77	1.15 ± 0.48
Total	$-$	2.55 ± 0.79	0.83 ± 1.77	2.55 ± 0.79

Table 8: Summary of QCD uncertainties $\Delta\sigma$ in the cross-sections and ΔA in the acceptances relative to the un-cut cross-section σ^{tot} for $M_{\ell\ell} > 40\,\text{GeV}/c^2$. The three cuts are described in table 2. Missing NNLO is shown with a sign, because it has been calculated.

These contributions to QCD errors are summarized in table 8 for the total cross-section and the three cuts of table 2. Results are shown both for the three cut cross-sections and their ratio for the total cross-section with $M_{\ell\ell} > 40\text{GeV}/c^2$, and the errors are assumed to be uncorrelated.

If the K-factor had not been calculated at NNLO, the error of the NLO cross-sections could have been roughly estimated from half the width of the scale-dependence band, or half the NLO results for $\Delta\sigma/\overline{\sigma}$ in table 5, giving uncertainties of $2.2 - 2.6\%$. The errors calculated from the K factors are in within the limits these expectations, up to the technical precision of the calculation. A similar error NLO estimate for the error in the acceptance based on table 6 would predict at most 0.33% missing NNLO. The actual missing NNLO in Cut 1 was found to be larger than this, but the other two cuts have very small missing NNLO, to within the technical precision of the calculation.

The final contribution to the total error considered here is the uncertainty from the PDFs. This may be extracted from the results of section 6 by taking the errors from the CTEQ6.5 results for Cut 1 (see table 2). The errors are asymmetric, so we take the largest of the two (up or down) uncertainties as the total fractional error for the PDF calculation. We choose the first cut set, since it is the most representative of likely analysis cuts at the LHC experiments. CTEQ errors, rather than the MRST errors, are used because they give a more conservative estimate. The difference between the results obtained by the latest CTEQ and MRST PDFs is less than the maximum error quoted for CTEQ for all three cut regions.

The errors are added in quadrature, assuming no correlations, and the results are given in table 9. It should be remarked that there is no concensus on the best way to combine the errors in table 9, so this total must be considered an estimate. The QCD error is taken for Cut 1 for the same reasons as given above. In addition, as we have discussed above, we propagate the "error on the error" for each of the contributions in order to have some reasonable estimate of the accuracy of the quoted total theoretical uncertainty.

Total Theoretical Uncertainty (%)

Uncertainty	Cross-section $\Delta\sigma$	Acceptance ΔA
Missing O(α) EWK	0.38 ± 0.26	0.96 ± 0.21
Total QCD Uncertainty	1.51 ± 0.75	2.55 ± 0.79
PDF Uncertainty	3.79	1.32
Total Uncertainty	4.1 ± 0.3	3.0 ± 0.7

Table 9: Total theoretical uncertainty on the Z production cross-section $\Delta\sigma$, and acceptances ΔA.

The exception to this is the PDF error, which can be considered as an upper limit on the uncertainty. We conclude that the event generator MC@NLO interfaced to PHOTOS should be sufficient to guarantee an overall theoretical uncertainty on the Z production due to higher order calculation, PDFs, and renormalization scale at the level of 4% for the total cross-section and at approximately 3% for the acceptance.

Z production will provide a valuable tool for studying QCD, measuring precision electroweak physics, and monitoring the luminosity. As the luminosity increases, the large statistics will permit a further improvement in the systematic uncertainties due to the PDFs. Adding complete O(α) EWK corrections to the event generator would eliminate most of the EWK uncertainty, and incorporating NNLO QCD corrections would substantially reduce the QCD uncertainties.

Reaching a combined precision of 1%, as desired in the later stages of analysis at high integrated luminosity, will require new tools. In addition to improved PDFs, an event generator combining NNLO QCD with complete O(α) EWK corrections will be needed, with exponentiation in appropriate regimes, and adequate convergence properties to technically reach the required precision. [27] Measurement strategies have been proposed that may mitigate some of the effects of systematic errors on the precision of the Z measurements. [2] A combination of improved calculations and improved meaurements will be needed to permit the desired precision to be reached as the integrated luminosity increases to a point where it is needed.
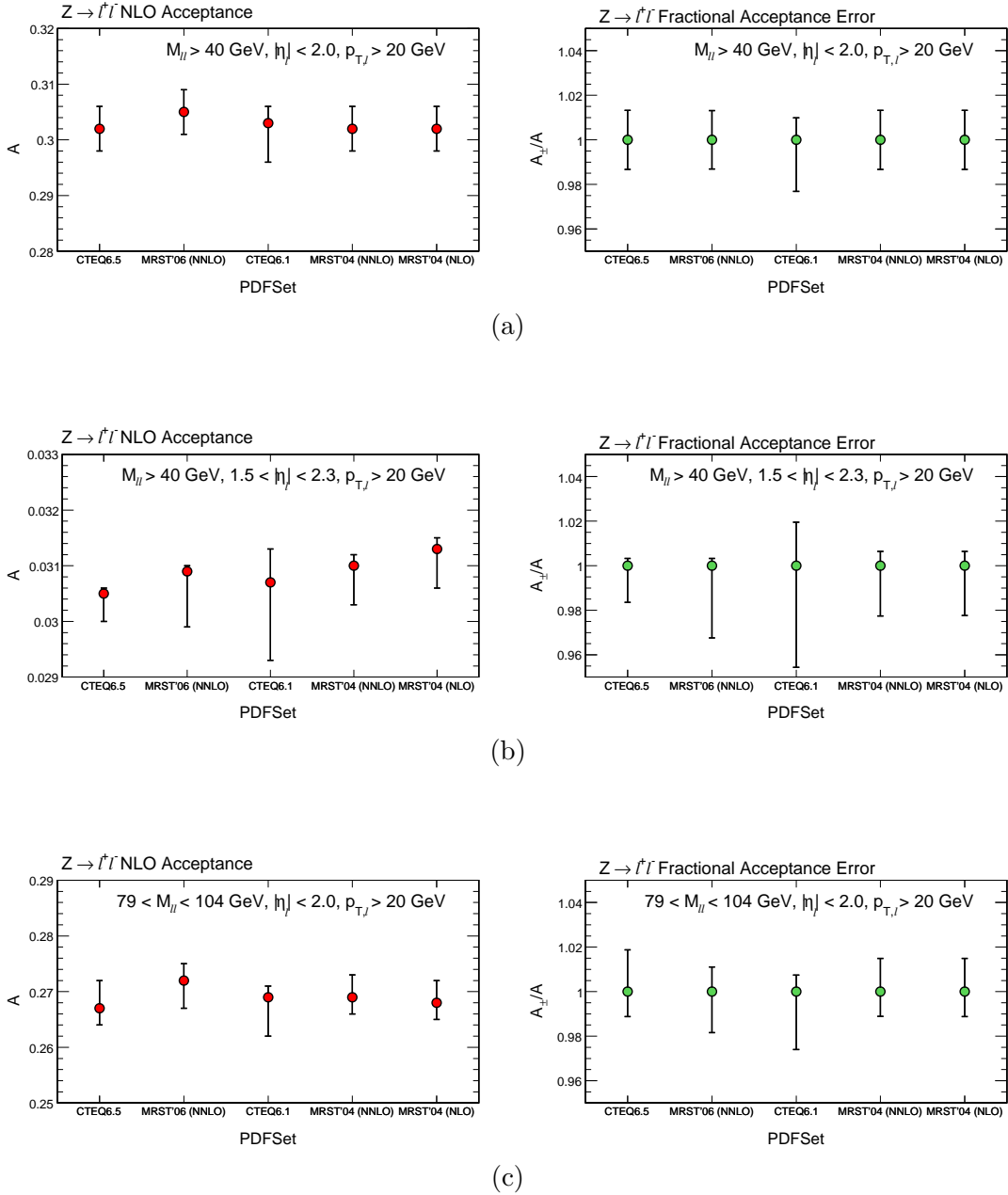
Acknowledgments

Figure 11: Comparison of $Z/\gamma^* \to \ell^+\ell^-$ ($\ell = e$ or μ) acceptances A, with several recent PDF calculations for acceptance regions (a) Cut 1, (b) Cut 2, and (c) Cut 3, as defined in table 2. The left-hand plots show the total acceptance and the right hand plots show the fractional error on the acceptance.
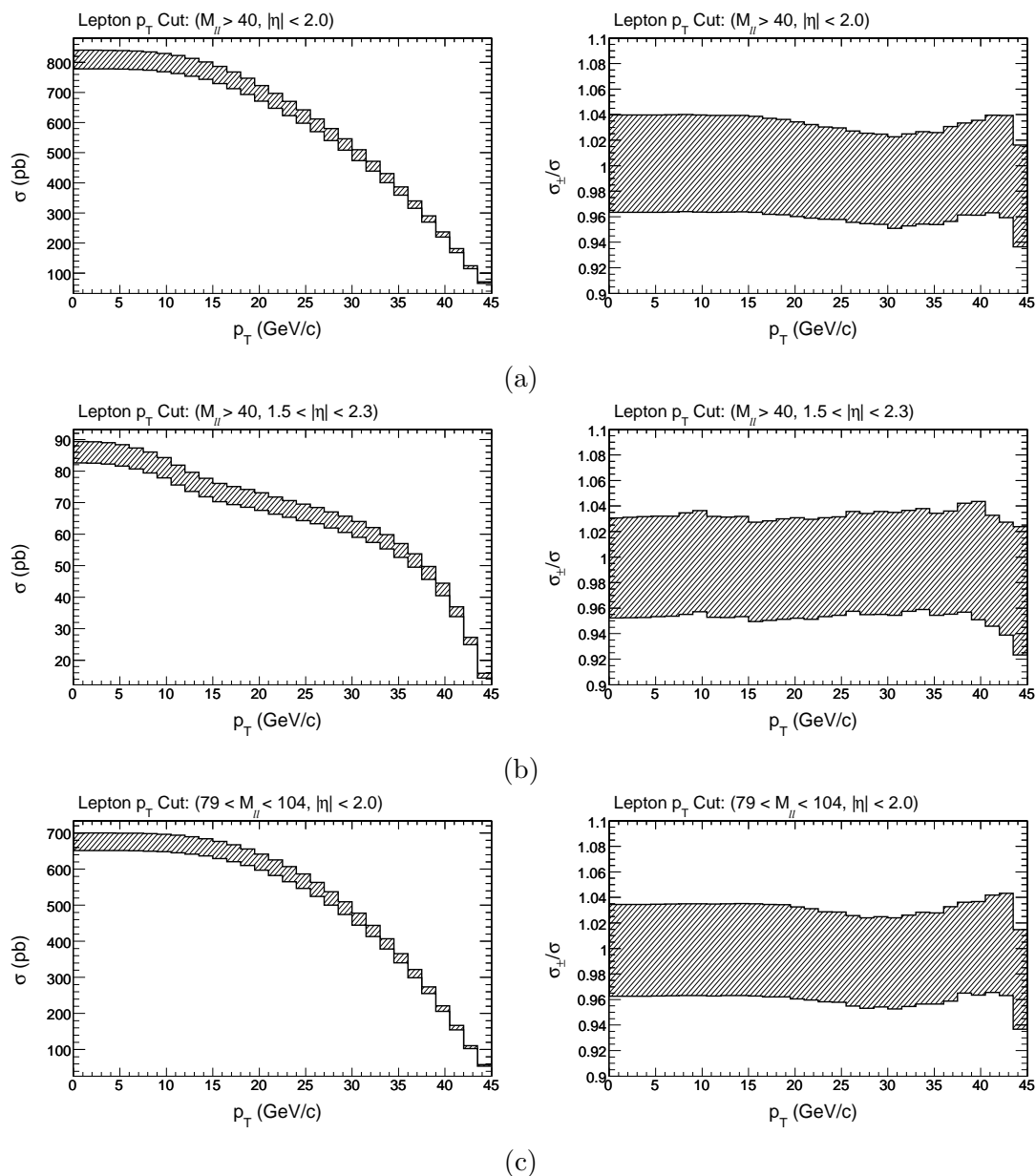
Figure 12: The $Z/\gamma^* \to \ell^+\ell^-$ cross-section σ ($\ell = e$ or μ), as a function of the p_{T} cut for acceptance regions (a) Cut 1, (b) Cut 2, and (c) Cut 3, as defined in table 2. For each acceptance region we fix the invariant mass and $|\eta|$ cuts at their specified values, and vary only the p_{T} cut. The figures on the right show the relative errors in the cross sections.
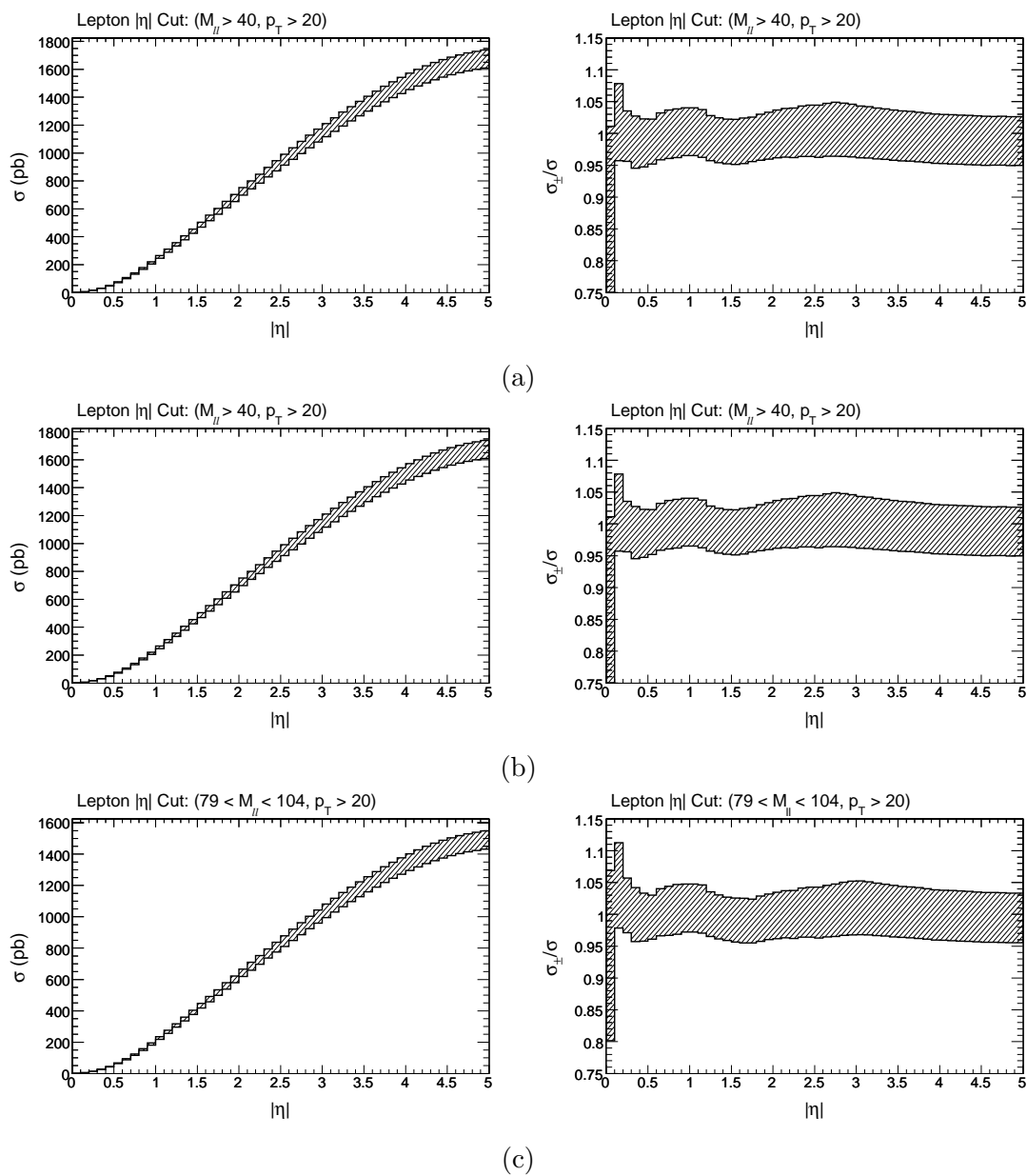
Figure 13: The $Z/\gamma^* \rightarrow \ell^+\ell^-$ cross-section σ ($\ell = e$ or μ), as a function of the $|\eta|$ cut for acceptance regions (a) Cut 1, (b) Cut 2, and (c) Cut 3, as defined in table 2. For each acceptance region we fix the invariant mass and p_{T} cuts at their specified values, and vary only the $|\eta|$ cut. The figures on the right show the relative errors in the cross sections.
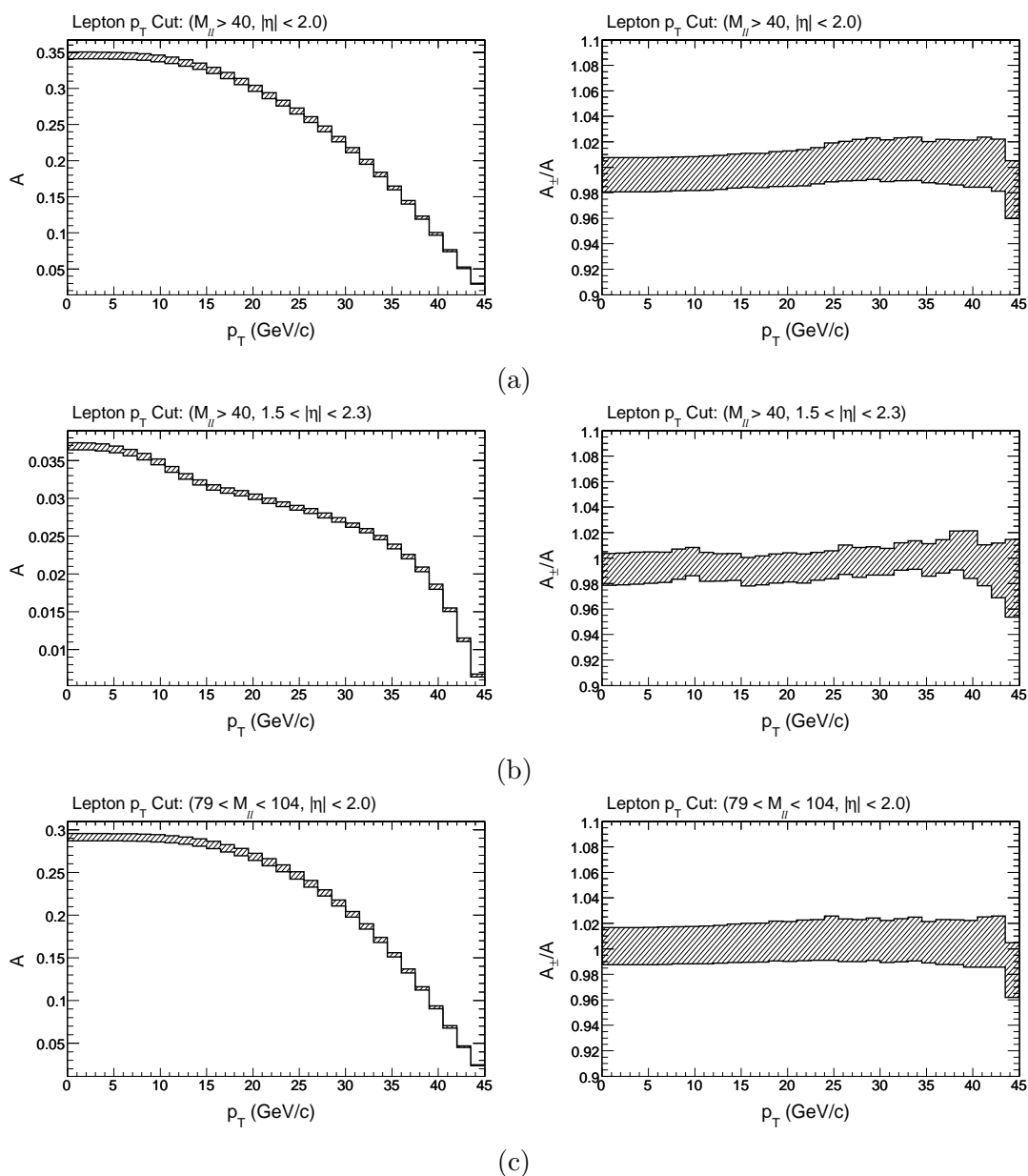
Figure 14: The $Z/\gamma^* \to \ell^+\ell^-$ acceptances A, as a function of the p_{T} cut for acceptance regions (a) Cut 1, (b) Cut 2, and (c) Cut 3, as defined in table 2. For each acceptance region we fix the invariant mass and $|\eta|$ cuts at their specified values, and vary only the p_{T} cut. The figures on the right show the relative errors in the acceptances.
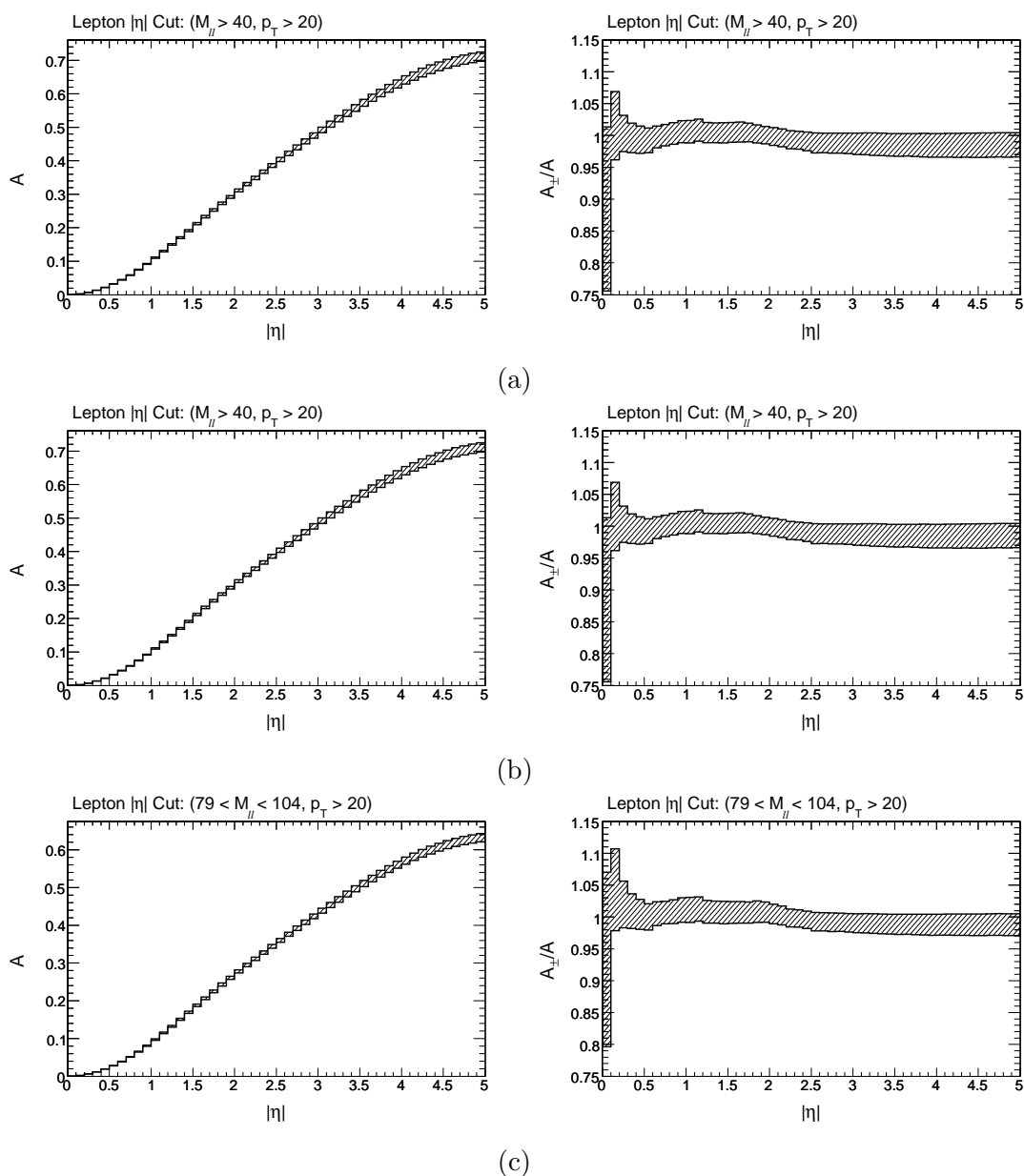
Figure 15: The $Z/\gamma^* \to \ell^+\ell^-$ acceptances A, as a function of the $|\eta|$ cut for acceptance regions (a) Cut 1, (b) Cut 2, and (c) Cut 3, as defined in table 2. For each acceptance region we fix the invariant mass and p_{T} cuts at their specified values, and vary only the $|\eta|$ cut. The figures on the right show the relative errors in the acceptances.

References

[1] M. Dittmar, F. Pauss and D. Zurcher, *Towards a precise parton luMINOSity determination at the CERN LHC*, *Phys. Rev.* **D 56** (1997) 7284 [`hep-ex/9705004`];
V.A. Khoze, A.D. Martin, R. Orava and M.G. Ryskin, *LuMINOSity monitors at the LHC*, *Eur. Phys. J.* **C 19** (2001) 313 [`hep-ph/0010163`];
W.T. Giele and S.A. Keller, *Hard scattering based luMINOSity measurement at hadron colliders*, `hep-ph/0104053`.

[2] M.W. Krasny, F. Fayette, W. Placzek and A. Siodmok, *Z-boson as 'the standard candle' for high precision W^- boson physics at LHC*, *Eur. Phys. J.* **C 51** (2007) 607 [`hep-ph/0702251`].

[3] S. Frixione and M.L. Mangano, *How accurately can we measure the W cross section?*, *JHEP* **05** (2004) 056 [`hep-ph/0405130`].

[4] R. Hamberg, W.L. van Neerven and T. Matsuura, *A complete calculation of the order alpha-S^2 correction to the Drell-Yan K factor*, *Nucl. Phys.* **B 359** (1991) 343 [*Erratum ibid.* **B 644** (2002) 403];
R.V. Harlander and W.B. Kilgore, *Next-to-next-to-leading order Higgs production at hadron colliders*, *Phys. Rev. Lett.* **88** (2002) 201801 [`hep-ph/0201206`].

[5] C. Anastasiou, L.J. Dixon, K. Melnikov and F. Petriello, *Dilepton rapidity distribution in the Drell-Yan process at NNLO in QCD*, *Phys. Rev. Lett.* **91** (2003) 182002 [`hep-ph/0306192`];
High-precision QCD at hadron colliders: electroweak gauge boson rapidity distributions at NNLO, *Phys. Rev.* **D 69** (2004) 094008 [`hep-ph/0312266`];
Vrap, www.slac.stanford.edu/∼lance/Vrap/.

[6] K. Melnikov and F. Petriello, *The W boson production cross section at the LHC through $O(\alpha_s^2)$*, *Phys. Rev. Lett.* **96** (2006) 231803 [`hep-ph/0603182`]; *Electroweak gauge boson production at hadron colliders through $O(\alpha_s^2)$*, *Phys. Rev.* **D 74** (2006) 114017 [`hep-ph/0609070`];
Higgs, W and Z boson production through NNLO in perturbative QCD, www-d0.fnal.gov/d0dist/dist/packages/melnikov_petriello/devel/FEHP.html.

[7] S.D. Drell and T.-M. Yan, *Massive lepton pair production in hadron-hadron collisions at high-energies*, *Phys. Rev. Lett.* **25** (1970) 316 [*Erratum ibid.* **25** (1970) 902].

[8] M. Bertini, L. Lönnblad and T. Sjöstrand, *PYTHIA version 7 − 0.0: a proof-of-concept version*, *Comput. Phys. Commun.* **134** (2001) 365 [`hep-ph/0006152`];
T. Sjöstrand et al., *High-energy-physics event generation with PYTHIA 6.1*, *Comput. Phys. Commun.* **135** (2001) 238 [`hep-ph/0010017`];
T. Sjöstrand, L. Lönnblad, S. Mrenna and P. Skands, *PYTHIA 6.3: physics and manual*, `hep-ph/0308153`;
T. Sjöstrand, S. Mrenna and P. Skands, *PYTHIA 6.4 physics and manual*, *JHEP* **05** (2006) 026 [`hep-ph/0603175`];
Present program version: PYTHIA, www.thep.lu.se/∼torbjorn/Pythia.html.

[9] G. Marchesini, B.R. Webber, G. Abbiendi, I.G. Knowles, M.H. Seymour and L. Stanco, *HERWIG: a Monte Carlo event generator for simulating hadron emission reactions with interfering gluons. Version 5.1 - April 1991*, *Comput. Phys. Commun.* **67** (1992) 465;
G. Corcella et al., *HERWIG 6: an event generator for hadron emission reactions with interfering gluons (including supersymmetric processes)*, *JHEP* **01** (2001) 010 [`hep-ph/0011363`]; *HERWIG 6.5 release note*, `hep-ph/0210213`;

S. Gieseke, A. Ribon, M.H. Seymour, P. Stephens and B. Webber, *Herwig++ 1.0: an event generator for e^+e^- annihilation*, *JHEP* **02** (2004) 005 [`hep-ph/0311208`];
HERWIG information, http://hepwww.rl.ac.uk/theory/seymour/herwig/.

[10] F.E. Paige, S.D. Protopopescu, H. Baer and X. Tata, *ISAJET 7.69: a Monte Carlo event generator for pp, $\bar{p}p$ and e^+e^- reactions*, `hep-ph/0312045`;
ISAJET a Monte Carlo event generator for p p, $\bar{p}p$, and e^+e^- Interactions, www.phy.bnl.gov/~isajet/.

[11] T. Gleisberg et al., *SHERPA 1.α, a proof-of-concept version*, *JHEP* **02** (2004) 056 [`hep-ph/0311263`];
A. Schalicke and F. Krauss, *Implementing the ME+PS merging algorithm*, *JHEP* **07** (2005) 018 [`hep-ph/0503281`];
C.-H. Chang, C.-F. Qiao, J.-X. Wang and X.-G. Wu, *Hadronic production of $B_c(B_c^*)$ meson induced by the heavy quarks inside the collision hadrons*, *Phys. Rev.* **D 72** (2005) 114009 [`hep-ph/0509040`]; *Simulating W/Z+jets production at the CERN LHC*, *Phys. Rev.* **D 72** (2005) 054017 [`hep-ph/0503280`];
Homepage of the sherpa event generator, http://projects.hepforge.org/sherpa/dokuwiki/doku.php.

[12] B.I. Ermolaev and V.S. Fadin, *Log-log asymptotic form of exclusive cross-sections in quantum chromodynamics*, *JETP Lett.* **33** (1981) 269 [*Pisma Zh. Eksp. Teor. Fiz.* **33** (1981) 285];
A.H. Mueller, *On the multiplicity of hadrons in QCD jets*, *Phys. Lett.* **B 104** (1981) 161;
A. Bassetto, M. Ciafaloni, G. Marchesini and A.H. Mueller, *Jet multiplicity and soft gluon factorization*, *Nucl. Phys.* **B 207** (1982) 189;
V.S. Fadin, *Double logarithmic asymptotics of the cross-sections of e^+e^- annihilation into quarks and gluons*, *Yad. Fiz.* **37** (1983) 408;
CDF collaboration, F. Abe et al., *Evidence for color coherence in $p\bar{p}$ collisions at $\sqrt{s} = 1.8\,TeV$*, *Phys. Rev.* **D 50** (1994) 5562;
D0 collaboration, B. Abbott et al., *Color coherent radiation in multijet events from $p\bar{p}$ collisions at $\sqrt{s} = 1.8\,TeV$*, *Phys. Lett.* **B 414** (1997) 419 [`hep-ex/9706012`].

[13] G. Altarelli, R.K. Ellis and G. Martinelli, *Large perturbative corrections to the Drell-Yan process in QCD*, *Nucl. Phys.* **B 157** (1979) 461;
P. Aurenche and J. Lindfors, *QCD corrections to direct lepton production in hadronic collisions*, *Nucl. Phys.* **B 185** (1981) 274.

[14] S. Frixione and B.R. Webber, *Matching NLO QCD computations and parton shower simulations*, *JHEP* **06** (2002) 029 [`hep-ph/0204244`];
S. Frixione, P. Nason and B.R. Webber, *Matching NLO QCD and parton showers in heavy flavour production*, *JHEP* **08** (2003) 007 [`hep-ph/0305252`];
The MC@NLO package, http://www.hep.phy.cam.ac.uk/theory/webber/MCatNLO/.

[15] E. Barberio, B. van Eijk and Z. Was, *PHOTOS: a universal Monte Carlo for QED radiative corrections in decays*, *Comput. Phys. Commun.* **66** (1991) 115;
E. Barberio and Z. Was, *PHOTOS: a universal Monte Carlo for QED radiative corrections. Version 2.0*, *Comput. Phys. Commun.* **79** (1994) 291;
P. Golonka and Z. Was, *PHOTOS Monte Carlo: a precision tool for QED corrections in Z and W decays*, *Eur. Phys. J.* **C 45** (2006) 97 [`hep-ph/0506026`];
Programs and papers by Zbigniew Was, http://wasm.web.cern.ch/wasm/goodies.html.

[16] P. Golonka and Z. Was, *Next to leading logarithms and the PHOTOS Monte Carlo*, *Eur. Phys. J.* **C 50** (2007) 53 [`hep-ph/0604232`].

[17] N.E. Adam, C.M. Carloni Calame, V. Halyo and C. Shepherd-Themistocleous, *Comparison of HORACE and PHOTOS in the $Z \to \ell^+\ell^-$ peak region*, to appear in Les Houches proceeding.

[18] C.M. Carloni Calame, G. Montagna, O. Nicrosini and M. Treccani, *Higher-order QED corrections to W-boson mass determination at hadron colliders*, Phys. Rev. **D 69** (2004) 037301 [hep-ph/0303102]; *Multiple photon corrections to the neutral-current Drell-Yan process*, JHEP **05** (2005) 019 [hep-ph/0502218];
C.M. Carloni Calame, G. Montagna, O. Nicrosini and A. Vicini, *Precision electroweak calculation of the charged current Drell-Yan process*, JHEP **12** (2006) 016 [hep-ph/0609170]; *Precision electroweak calculation of the production of a high transverse-momentum lepton pair at hadron colliders*, JHEP **10** (2007) 109 [arXiv:0710.1722];
Horace event generator home page, http://www.pv.infn.it/~hepcomplex/horace.html.

[19] Q.-H. Cao and C.P. Yuan, *Combined effect of QCD resummation and QED radiative correction to W boson observables at the Tevatron*, Phys. Rev. Lett. **93** (2004) 042001 [hep-ph/0401026];
C. Balázs and C.P. Yuan, *Soft gluon effects on lepton pairs at hadron colliders*, Phys. Rev. **D 56** (1997) 5558 [hep-ph/9704258];
C. Balázs, J.-w. Qiu and C.P. Yuan, *Effects of QCD resummation on distributions of leptons from the decay of electroweak vector bosons*, Phys. Lett. **B 355** (1995) 548 [hep-ph/9505203];
G.A. Ladinsky and C.P. Yuan, *The nonperturbative regime in QCD resummation for gauge boson production at hadron colliders*, Phys. Rev. **D 50** (1994) 4239 [hep-ph/9311341];
Q_T *resummation portal at Michigan state university*, http://hep.pa.msu.edu/resum/.

[20] U. Baur, S. Keller and W.K. Sakumoto, *QED radiative corrections to Z boson production and the forward backward asymmetry at hadron colliders*, Phys. Rev. **D 57** (1998) 199 [hep-ph/9707301];
U. Baur, O. Brein, W. Hollik, C. Schappacher and D. Wackeroth, *Electroweak radiative corrections to neutral-current Drell-Yan processes at hadron colliders*, Phys. Rev. **D 65** (2002) 033007 [hep-ph/0108274].

[21] W.K. Tung et al., *Heavy quark mass effects in deep inelastic scattering and global QCD analysis*, JHEP **02** (2007) 053 [hep-ph/0611254];
D. Stump et al., *Inclusive jet production, parton distributions and the search for new physics*, JHEP **10** (2003) 046 [hep-ph/0303013];
J. Pumplin et al., *New generation of parton distributions with uncertainties from global QCD analysis*, JHEP **07** (2002) 012 [hep-ph/0201195];
CTEQ6 parton distribution functions,
http://hep.pa.msu.edu/people/wkt/cteq6/cteq6pdf.html.

[22] C. Anastasiou, G. Dissertori and F. Stockli, *NNLO QCD predictions for the $H \to WW \to ll\nu\nu$ signal at the LHC*, JHEP **09** (2007) 018 [arXiv:0707.2373];
C. Anastasiou, G. Dissertori, F. Stockli and B.R. Webber, *QCD radiation effects on the $H \to WW \to l\nu l\nu$ signal at the LHC*, JHEP **03** (2008) 017 [arXiv:0801.2682].

[23] G.P. Lepage, *A new algorithm for adaptive multidimensional integration*, J. Comput. Phys. **27** (1978) 192;
T. Hahn, *CUBA: a library for multidimensional numerical integration*, Comput. Phys. Commun. **168** (2005) 78 [hep-ph/0404043].

[24] A.D. Martin, W.J. Stirling, R.S. Thorne and G. Watt, *Update of parton distributions at NNLO*, Phys. Lett. **B 652** (2007) 292 [arXiv:0706.0459]; *MRST partons generated in a fixed-flavour scheme*, Phys. Lett. **B 636** (2006) 259 [hep-ph/0603143];

A.D. Martin, R.G. Roberts, W.J. Stirling and R.S. Thorne, *Uncertainties of predictions from parton distributions. I: experimental errors*, *Eur. Phys. J.* **C 28** (2003) 455 [hep-ph/0211080]; *MRST*2001: *partons and α_s from precise deep inelastic scattering and Tevatron jet data*, *Eur. Phys. J.* **C 23** (2002) 73 [hep-ph/0110215]; *Estimating the effect of NNLO contributions on global parton analyses*, *Eur. Phys. J.* **C 18** (2000) 117 [hep-ph/0007099];
MRST parton distributions, http://durpdg.dur.ac.uk/hepdata/mrs.html.

[25] A. Cafarella, C. Corianò and M. Guzzi, *NNLO logarithmic expansions and precise determinations of the neutral currents near the Z resonance at the LHC: the Drell-Yan case*, *JHEP* **08** (2007) 030 [hep-ph/0702244]; *NNLO logarithmic expansions and exact solutions of the DGLAP equations from x-space: new algorithms for precision studies at the LHC*, *Nucl. Phys.* **B 748** (2006) 253 [hep-ph/0512358].

[26] P.M. Nadolsky and Z. Sullivan, *PDF uncertainties in W H production at Tevatron*, *eConf* **C010630** (2001) P510 [hep-ph/0110378].

[27] C. Glosser, S. Jadach, B.F.L. Ward and S.A. Yost, *QED $\otimes$ QCD threshold corrections at the LHC*, *Mod. Phys. Lett.* **A 19** (2004) 2113 [hep-ph/0404087];
B.F.L. Ward et al., *New results on precision studies of heavy vector boson physics*, *Int. J. Mod. Phys.* **A 20** (2005) 3258 [hep-ph/0411051];
B.F.L. Ward and S.A. Yost, *QED $\otimes$ QCD resummation and shower/ME matching for LHC physics*, *Acta Phys. Polon.* **B38** (2007) 2395 [arXiv:0704.0294]; *New developments in precision LHC theory: qEDXQCD exponentiation, shower/ME matching, IR-improved DGLAP-CS theory and implications for UV finite quantum gravity*, arXiv:0802.0724.